On Segmenting Pupil Contours in Terms of Elliptical Fourier Series

Supplementary Information

Felix O'Mahony
Pupil Labs
Berlin, Germany
flx@pupil-labs.com

Patrick Fürst
Pupil Labs
Berlin, Germany
pfu@pupil-labs.com

Michael Drews
Pupil Labs
Berlin, Germany
mic@pupil-labs.com

Kai Dierkes
Pupil Labs
Berlin, Germany
kai@pupil-labs.com

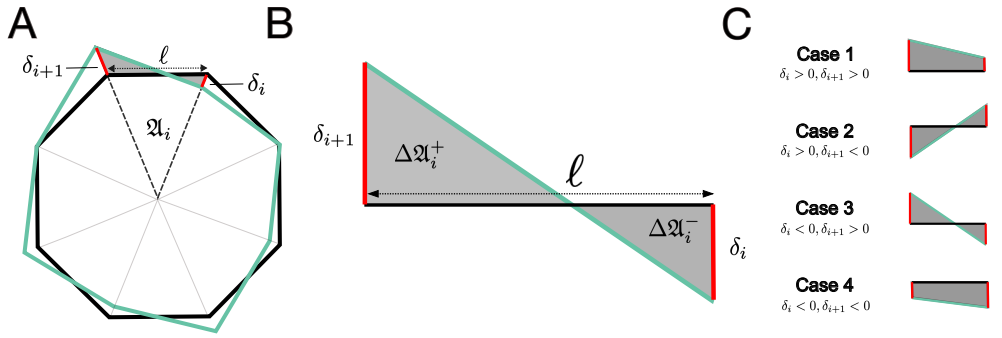

Figure S1. **Derivation of Approximate Expressions of the Expected IoU and Its Variance. (A)**: An idealized pupil consists of identical triangular segments, each of area $\mathfrak{A}_i = \mathfrak{A}/n$, where n is the number of vertices. Given a simulated segmentation (green polygon), each triangular segment is perturbed along its spokes by δ_i and δ_{i+1} (red lines). **(B)**: Approximating the spokes as parallel allows for calculating the areas of $\mathfrak{A}_i^+$ and $\mathfrak{A}_i^+$ as a function of δ_i and δ_{i+1}. **(C)**: Depending on the sign of δ_i and δ_{i+1}, four cases of equal probability need to be treated separately. Examples of all four cases are shown.

A. Derivation of IoU Statistics

In the framework of the geometric model of an idealized pupil and its segmentations (introduced in Section 4.2), we derive expressions for the expectation value, $\mathbb{E}_{\text{IoU}}$, and the variance, Var(IoU), as a function of area ($\mathfrak{A}$) and boundary error (σ).

A.1. Expected IoU

To this end, assume we are presented with a ground-truth pupil polygon with area $\mathfrak{A}$ and number of vertices n. We consider an individual triangular segment of the ground-truth pupil, defined by the centroid and two adjacent vertices (see Fig. S1A). Let the area of the triangle be denoted by $\mathfrak{A}_i$, and the length of its exterior edge, i.e. the edge connecting the two vertices, by ℓ. For a randomly drawn segmentation, the corresponding triangular segment is obtained by displacing the two ground-truth vertices by $\delta_i \sim \mathcal{N}(0, \sigma)$ and $\delta_{i+1} \sim \mathcal{N}(0, \sigma)$ in the radial direction. This results in either two triangles formed with the exterior edge if δ_i and δ_{i+1} are of opposite sign (grey shaded regions in Fig. S1A), or a trapezium if they are of the same sign (see Fig. S1C for a depiction of all cases).

We further make the simplifying approximation that the two spokes of the triangular segment are parallel to each other (see Fig. S1B). This is justified when ℓ is much smaller than the diameter of the segmentation, which e.g. is the case when the number of vertices n is large. We denote the area of the shaded region lying outside of the ground-truth shape as $\mathfrak{A}_i^+$, the area of the interior shaded region as $\mathfrak{A}_i^-$. Note, that one of these two areas can be zero (Case 1 and Case 4). We can then calculate $\mathfrak{A}_i^+$ and $\mathfrak{A}_i^-$ in terms of the perturbations δ_i and δ_{i+1} for each of the four sign combinations of δ_i and δ_{i+1}.

Case 1: $\delta_i > 0, \delta_{i+1} > 0$:

$$\mathfrak{A}_i^+ = \frac{1}{2}(\delta_i + \delta_{i+1})\ell \tag{S1}$$

$$\mathfrak{A}_i^- = 0 \tag{S2}$$

Case 2: $\delta_i > 0$, $\delta_{i+1} < 0$:

$$\mathfrak{A}_i^+ = \frac{1}{2}\frac{\delta_i^2}{\delta_i - \delta_{i+1}}\ell \tag{S3}$$

$$\mathfrak{A}_i^- = \frac{1}{2}\frac{\delta_{i+1}^2}{\delta_i - \delta_{i+1}}\ell \tag{S4}$$

Case 3: $\delta_i < 0$, $\delta_{i+1} > 0$:

$$\mathfrak{A}_i^+ = \frac{1}{2}\frac{\delta_{i+1}^2}{\delta_{i+1} - \delta_i}\ell \tag{S5}$$

$$\mathfrak{A}_i^- = \frac{1}{2}\frac{\delta_i^2}{\delta_{i+1} - \delta_i}\ell \tag{S6}$$

Case 4: $\delta_i < 0$, $\delta_{i+1} < 0$:

$$\mathfrak{A}_i^+ = 0 \tag{S7}$$

$$\mathfrak{A}_i^- = -\frac{1}{2}(\delta_i + \delta_{i+1})\ell \tag{S8}$$

In each of the four cases, δ_i and δ_{i+1} follow a half-normal distribution (as their sign is fixed). The mean of this half-normal distribution is given by $\mu = \sqrt{2/\pi}\sigma$. We can therefore calculate/approximate the expectation values $\mathbb{E}(\mathfrak{A}_i^+)$ and $\mathbb{E}(\mathfrak{A}_i^-)$ for each case by substituting μ into the equations above, leading to:

Case 1: $\delta_i > 0$, $\delta_{i+1} > 0$:

$$\mathbb{E}(\mathfrak{A}_i^+) = \sqrt{\frac{2}{\pi}}\sigma\ell \tag{S9}$$

$$\mathbb{E}(\mathfrak{A}_i^-) = 0 \tag{S10}$$

Case 2: $\delta_i > 0$, $\delta_{i+1} < 0$:

$$\mathbb{E}(\mathfrak{A}_i^+) \approx \frac{1}{2\sqrt{2\pi}}\sigma\ell \tag{S11}$$

$$\mathbb{E}(\mathfrak{A}_i^-) \approx \frac{1}{2\sqrt{2\pi}}\sigma\ell \tag{S12}$$

Case 3: $\delta_i < 0$, $\delta_{i+1} > 0$:

$$\mathbb{E}(\mathfrak{A}_i^+) \approx \frac{1}{2\sqrt{2\pi}}\sigma\ell \tag{S13}$$

$$\mathbb{E}(\mathfrak{A}_i^-) \approx \frac{1}{2\sqrt{2\pi}}\sigma\ell \tag{S14}$$

Case 4: $\delta_i < 0$, $\delta_{i+1} < 0$:

$$\mathbb{E}(\mathfrak{A}_i^+) = 0 \tag{S15}$$

$$\mathbb{E}(\mathfrak{A}_i^-) = \sqrt{\frac{2}{\pi}}\sigma\ell \tag{S16}$$

In order to calculate the IoU of a given segmentation with respect to the ground-truth pupil, note that $\mathfrak{A}_i^+$ increases the size of the union of the two shapes, while $\mathfrak{A}_i^-$ reduces the size of the intersection of the two shapes. The total increase of the union is therefore the sum of all $\mathfrak{A}_i^+$, the total reduction of the intersection the sum of all $\mathfrak{A}_i^-$. Thus, the expected IoU can be expressed as:

$$\mathbb{E}(\text{IoU}) = \mathbb{E}\left(\frac{\mathfrak{A} - \sum_{i=1}^{n} \mathfrak{A}_\text{i}^-}{\mathfrak{A} + \sum_{i=1}^{n} \mathfrak{A}_\text{i}^+}\right) \approx \frac{\mathfrak{A} - \sum_{i=1}^{n} \mathbb{E}(\mathfrak{A}_\text{i}^-)}{\mathfrak{A} + \sum_{i=1}^{n} \mathbb{E}(\mathfrak{A}_\text{i}^+)}. \tag{S17}$$

As each of the four cases occurs with equal probability, i.e. $\frac{1}{4}$, the expected IoU, using Eqs. (S9-S16), can be expressed as:

$$\mathbb{E}(\text{IoU}) = \frac{\mathfrak{A} - n\frac{1}{4}\sqrt{\frac{2}{\pi}}\sigma\ell - n\frac{1}{2}\frac{1}{2\sqrt{2\pi}}\sigma\ell}{\mathfrak{A} + n\frac{1}{4}\sqrt{\frac{2}{\pi}}\sigma\ell + n\frac{1}{2}\frac{1}{2\sqrt{2\pi}}\sigma\ell}. \tag{S18}$$

Approximating the ground-truth pupil as a circle, ℓ can be further expressed in terms of $\mathfrak{A}$ and n as

$$\ell = \sqrt{\frac{4\mathfrak{A}\pi}{n}}. \tag{S19}$$

We now substitute Eq. (S19) into Eq. (S18) to arrive at the final expression, approximating the dependence of expected IoU as a function of area and boundary error:

$$\mathbb{E}(\text{IoU}) \approx \frac{\mathfrak{A} - \sqrt{\frac{9\mathfrak{A}}{8}}\sigma}{\mathfrak{A} + \sqrt{\frac{9\mathfrak{A}}{8}}\sigma}. \tag{S20}$$

Note, in particular, that this expression does not depend on the choice of n.

A.2. Variance of IoU

In order to derive an expression for the variance of the IoU, we consider the IoU of a single triangular segment of the idealized pupil, i.e.

$$\text{IoU}_i(\delta_i, \delta_{i+1}) = \frac{\mathfrak{A}_i - \mathfrak{A}_i^-(\delta_i, \delta_{i+1})}{\mathfrak{A}_i + \mathfrak{A}_i^+(\delta_i, \delta_{i+1})}. \tag{S21}$$

The variance of IoU_i is then given by

$$\text{Var}(\text{IoU}_i) = \int_{-\infty}^{\infty}\int_{-\infty}^{\infty}\left(\frac{\mathfrak{A} - \mathfrak{A}_i^-(\delta_i, \delta_{i+1})}{\mathfrak{A} + \mathfrak{A}_i^+(\delta_i, \delta_{i+1})} - \mathbb{E}(\text{IoU}_i)\right)^2 p(\delta_i)p(\delta_{i+1})d\delta_i d\delta_{i+1},$$

where p is the probability density of a univariate normal distribution with zero mean and standard deviation σ. While the resulting integral is not soluble analytically, it can be calculated numerically.

Finally, we note that a polygon with n sides has $n/2$ independent triangular regions (since one perturbation δ_i is shared by two polygon segments), and so the net variance can be approximated by:

$$\text{Var}(\text{IoU}) \approx \frac{2\text{Var}(\text{IoU}_i)}{n}. \tag{S22}$$

Unlike the approximation for the expected IoU, Eq. (S22) not only contains the area $\mathfrak{A}$ and the boundary error σ, but also depends on the number of vertices n.

Note, by simply taking the square root of the right-hand side, Eq. (S22) also provides an estimate for the standard deviation of the IoU.

A.3. Comparison to Simulation

We validate the derived expressions for the expected IoU and its variance by means of numerical simulation. Specifically, for a set of values for $\mathfrak{A}$ and σ, we simulate the corresponding IoU distribution by randomly generating segmentations based on the geometric model and calculate both the corresponding expectation value as well as variance. We then compare these numerical outcomes to the theoretical predictions given by Eq. (S20) and Eq. (S22). The results, presented in Fig. S2, demonstrate a close alignment between the derived expressions and the numerical simulations.

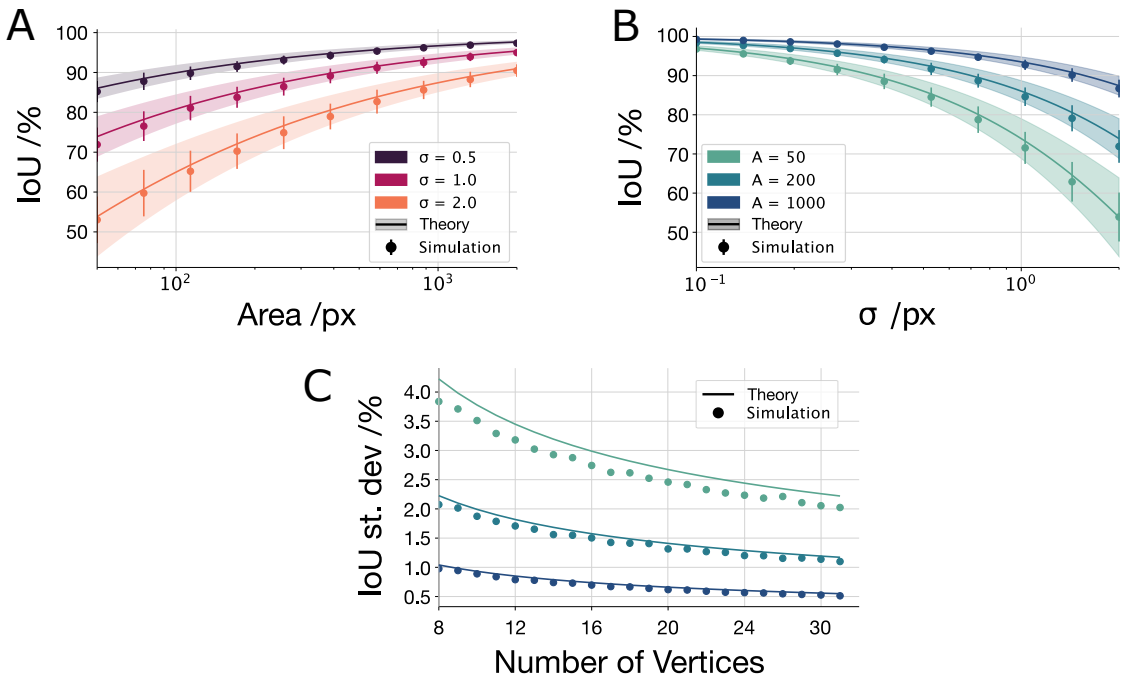

Figure S2. **Theory vs. Simulation.** **(A)**: Numerical simulation of IoU distributions as a function of area $\mathfrak{A}$ at several values of boundary error σ. Points correspond to the expectation value, vertical lines extend one standard deviation above and below the expectation value. We compare to theoretical predictions according to Eq. (S20) and Eq. (S22): lines correspond to the expectation value, shaded regions extend one standard deviation above and below the expectation value. **(B)**: IoU as a function of σ at several values of area $\mathfrak{A}$. **C**: Standard deviation of IoU as a function of number of vertices n at several values of area $\mathfrak{A}$ for a fixed value of $\sigma = 0.5$.

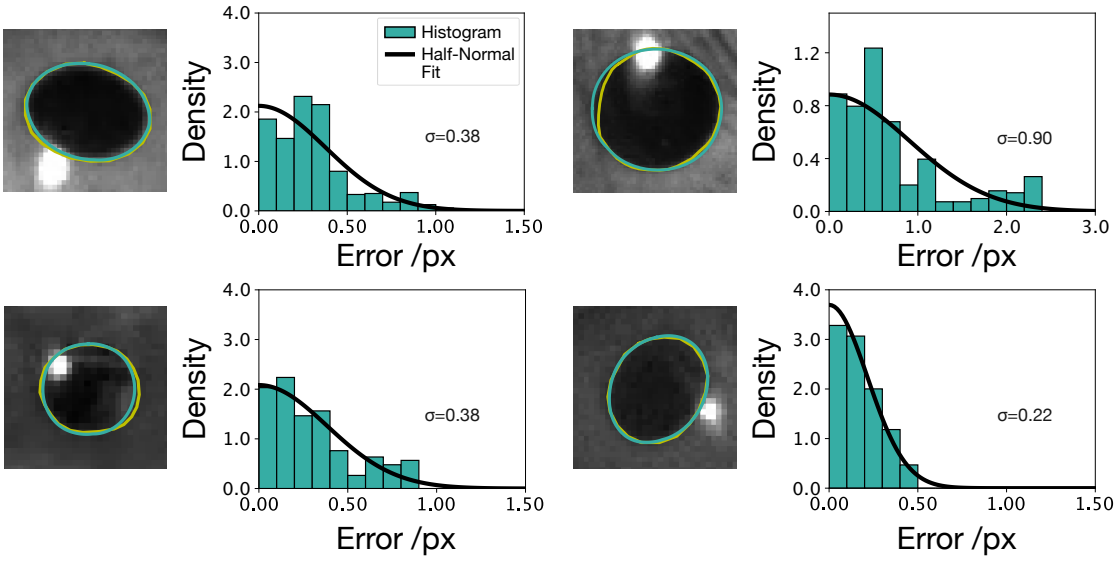

Figure S3. **Examples of Half-Normal Fitting to Individual Segmentation Results.** The displayed images are selected from the validation dataset, with ground-truth labels shown in yellow and EFNet segmentations depicted in green. Corresponding histograms illustrate the distribution of absolute deviations from EFNet segmentations to the ground-truth, while the black curves represent the fitted half-normal distributions. Corresponding estimates of σ are given in each panel.

B. Estimation of Boundary Error

In Fig. S3, we present four examples of sample-wise distributions of the absolute radial distance $|\delta(\phi)|$ between the respective EFNet predictions and the ground-truth segmentations. Fits of half-normal distributions parametrized by σ are overlaid as black lines. The values of σ corresponding to these fits provide the sample-wise estimates of the boundary error.

C. Upsampling by Temporal Interpolation of Fourier Modes

One notable advantage of the proposed method lies in its capacity to interpolate segmentations over time in a straightforward manner. This capability is illustrated in Fig. S4. Using a Neon recording approximately 6 s long and captured at 200 Hz, we obtained segmentations by EFNet on each individual eye image. In panel A, we display a subset of the evolution of the predicted Fourier coefficients over time, demonstrating their smooth variation. Values are z-scored. Changes in gaze direction or pupil size result in smooth changes of the corresponding Fourier coefficients. In scenarios where e.g. computational constraints prevent segmentation of every frame, the proposed method enables straightforward interpolation between frames. This is exemplified for the pink-shaded region of the timeline in panel C, where we linearly interpolate the Fourier coefficients using their values at the black vertical markers to generate segmentations for intermediate time points. As illustrated by the comparison between Fig. S4B and Fig. S4C, the interpolated segmentations closely match the EFNet outputs achieved at the full temporal resolution.

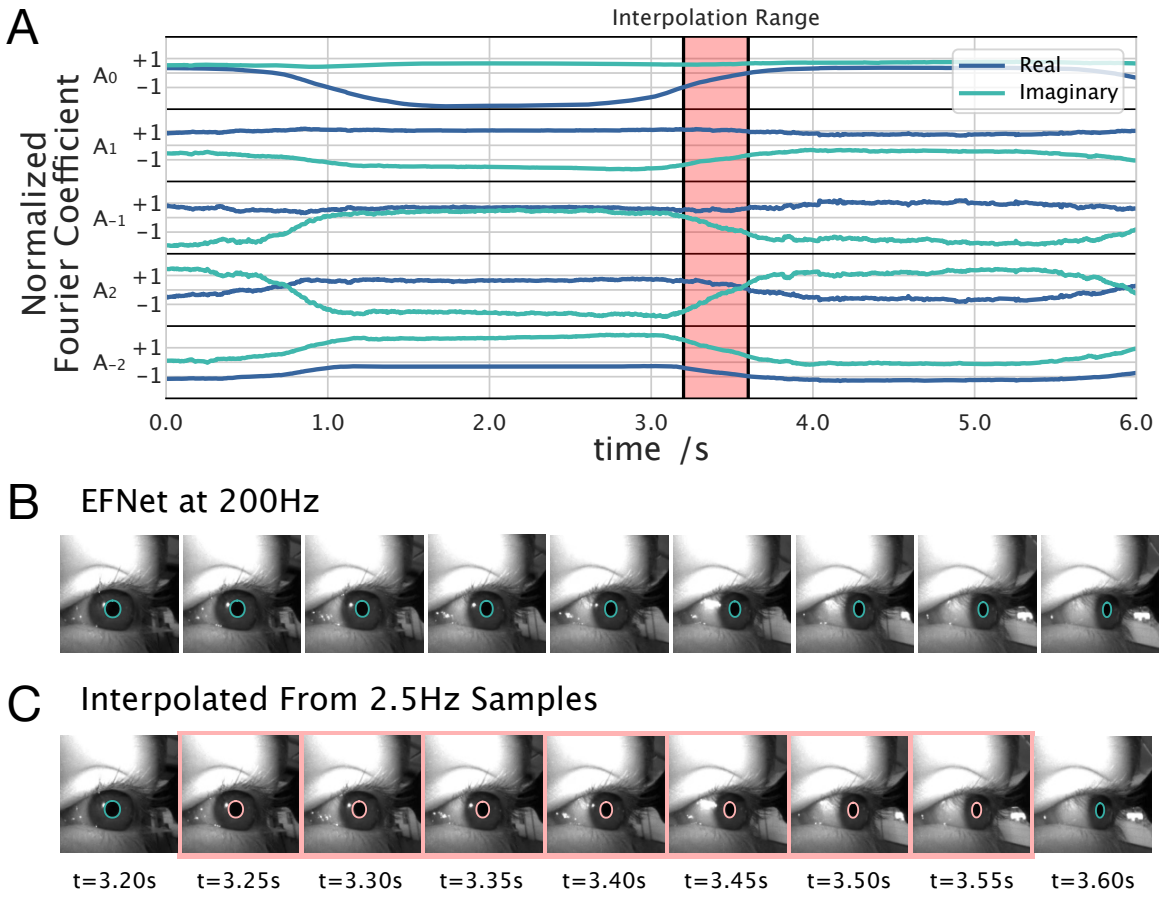

Figure S4. **Temporal Interpolation of Segmentations. (A)** We show z-scored trajectories of the first five Fourier coefficients obtained by a frame-by-frame EFNet-segmentation of a 6 s Neon recording. Note the smooth variation of the coefficients over time. **(B)** We show corresponding segmentations for an eye rotation occuring over the period shaded in red in panel A. **(C)** Linearly interpolating the values at the boundaries of the red shaded region (corresponding to an effective sampling rate of 2.5 Hz), we obtain alternative segmentations for the time points in between. Note the favourable comparison of the corresponding segmentations shown in B and C.

D. IoU and Boundary Error of Fourier Fits

We calculated IoU scores for the segmentations obtained by directly fitting the proposed parametrization (Eq.(1) in the main text) to our validation set. The resulting mean IoUs are summarized in Table S1. For $N \leq 8$, increasing the number of Fourier modes leads to appreciable improvements in the mean IoU scores. However, the returns diminish for larger values of N, indicating that higher-order modes contribute minimally to pupil shape. Notably, for $N = 8$, the fits almost perfectly capture the ground-truth annotations, achieving IoU scores close to 1.

N	IoU	Boundary Error
1	0.963	0.210
2	0.974	0.151
4	0.986	0.088
6	0.990	0.065
8	0.992	0.054
10	0.993	0.047
12	0.994	0.043
16	0.995	0.037

Table S1. **Mean IoU and Boundary Error for Fits of Ground-Truth Annotations by Eq. (1) for Increasing N.**